RSC Advances

REVIEW

View Article Online
View Journal | View Issue

Cite this: *RSC Adv.*, 2017, **7**, 47886

Recent developments in graphene-based/nanometal composite filter membranes

Meng-meng Cheng,[a] Lin-jun Huang,*[a] Yan-xin Wang,[a] Jian-guo Tang,*[a] Yao Wang,[a] Yun-chao Zhao,[a] Gui-fei Liu,[a] Yang Zhang,[a] Matt J. Kipper,[b] Laurence A. Belfiore[b] and Wickramasinghe S. Ranil[c]

Significant achievements have been made in the development of next-generation filtration and separation membranes using graphene materials; graphene-based membranes are promising in many areas, such as membrane separation, water desalination, proton conductors, and energy storage and conversion. In recent years, based on the excellent barrier and permeability of graphene sheets, researchers have conducted considerable research on graphene-based composite filter membranes and have made great progress. In this review paper, we summarize the key research contributions in graphene-based/nanometal composite membranes, analyze the existing problems, and elaborate on the potential application in water treatment and development trend of this kind of membrane. Graphene-based/nanometal composite membranes not only have good antibacterial activity and adsorbability, but also have potential application in seawater desalination and sewage treatment. Therefore, we can foresee that graphene-based/nanometal composite membranes will play an important role in water treatment. This review will serve as a valuable platform to fully understand filtration and adsorption mechanism through graphene-based membranes as well as the latest progress in graphene-based/nanometal composite filter membranes.

Received 22nd July 2017
Accepted 26th September 2017

DOI: 10.1039/c7ra08098k

rsc.li/rsc-advances

1. Introduction

Since the beginning of the twenty-first century, water resources have become an important factor restricting the development of a country or region due to growing population and industrial demand. According to statistics, at present, 1/3 of the world's population live in water-scarce areas, and this ratio is likely to reach 2/3 by 2025. The shortage of water resources is likely to become even more severe and complicated because of population expansion, industrialization, climate change and increasing water pollution.[1] Therefore, how to ensure the supply of water for people's livelihood and industry has become a major issue related to the national economy and people's livelihood, and even to national security.

Membrane separation technology is a kind of technology that uses a selective separation membrane to separate the mixture under external force. Different from other water treatment methods (adsorption, distillation, *etc.*), membrane separation technology has many advantages, such as the absence of chemical additives, heat input and regeneration of adsorption medium.[2] Therefore, the development of separation membrane and membrane separation technology is an important way to solve existing water resources problems. Nanofiltration (NF) membrane is a pressure-driven and liquid-phase separation membrane with molecular weight between 200 and 1000. It first appeared commercially around 1985 and was widely available by the 1990s.[3] After nearly 30 years of development, NF membrane and NF separation technology have been widely used in food and chemical industry, pharmaceutical industry, waste-water treatment, desalination industry and other fields.[4–10] In addition to the field of water treatment, NF membrane can also be applied to organic phases and for liquid-phase separation processes based on ionic liquids.[11] But because of the innate limitations of traditional polymers and inorganic membranes, the development of NF membrane has encountered many problems, such as low separation efficiency, anti-fouling and chlorine resistance, in order to overcome these problems, nanotechnology has been applied to the fields of NF membrane in recent research.

Graphene is made of carbon atoms and it is a two-dimensional graphite crystal. Graphene was discovered in 2004 and the Andre Geim[12] research group won the 2010 Nobel Prize in Physics for this important discovery; they used the micro-mechanical peeling method to obtain the first piece of graphene in the world. Graphene has many amazing properties, such as good mechanical properties,[13] high surface area[14,15] and

[a]*Institute of Hybrid Materials, National Center of International Research for Hybrid Materials Technology, National Base of International Science & Technology Cooperation, College of Materials Science and Engineering, Qingdao University, Qingdao 266071, P. R. China. E-mail: newboy66@126.com; tang@qdu.edu.cn; Fax: +86 532 85951519; Tel: +86 532 85951961*

[b]*Department of Chemical and Biological Engineering, Colorado State University, Fort Collins, CO 80523, USA*

[c]*Ralph E. Martin Department of Chemical and Engineering, University of Arkansas, Fayetteville, AR 72703, USA*

quantum Hall effect[16–19] and superconductivity.[20–22] In addition, graphene has good barrier properties to gases and liquids, and water exhibits a low friction flow between confined graphene layers. Therefore, membrane materials assembled by graphene or graphene oxide exhibit good separation, which makes graphene-based materials have a very expansive application prospect in the field of membrane separation.

2. Structure of graphene materials

2.1. Structure of graphene

Graphene is a two-dimensional sheet of sp^2-bonded carbon atoms in a hexagonal honeycomb lattice with atomic thickness, as shown in Fig. 1. Besides, as we can see in Fig. 2, graphene is a basic building block for graphitic materials of all other dimensionalities.[23]

Graphene possesses chemical features similar to CNTs but with structural variation wherein it can be considered as a planar version of its tubular counterpart. The revolutionary discovery of the "thinnest" known material graphene has added a new dimension of research in the fields of physics, chemistry, biotechnology, and materials science.[24] Graphene is endowed with a large theoretical specific surface area of 2630 $m^2\ g^{-1}$ and hydrophobic nature.[25] However, the prevention of aggregation is essential for graphene sheets as most of their unique properties are only associated with individual sheets.[26] Previously, graphene has been mostly explored in the physical field for application in photovoltaic devices, photocatalysis and sensors because their surfaces are chemically inert.[27–29] Recently, the possible applications of graphene-based materials have rapidly expanded to other areas such as environmental remediation.[30] For molecular separation processes, computational simulation predicts that graphene-based membrane demonstrates a great potential for molecular separation.[31,32] As a result, graphene has been favorably used as alternative carbon-based nanofiller in the preparation of polymer nanocomposites with improved mechanical, thermal, and electrical properties because of graphene's layer structure.[33–36]

2.2. Structure of nanoporous graphene

Nanoporous graphene (NG) membrane can be obtained by introducing nanopores on the surface of graphene. Du *et al.*[37] designed a series of NG membranes of different sizes and shapes; NG membranes can separate N_2 and H_2 according to different gas permeation mechanisms, as shown in Fig. 3(a). Sint *et al.*[38] designed nanopores with different functional groups on the basis of graphene nanosheets, as we can see in Fig. 3(b). It is found that graphene nanosheets have high ionic selectivity according to molecular dynamics simulation. So, NG can be regarded as a good ion sieve material. Besides, Cohen-Tanugi and Grossman[39] also simulated functional monolayer graphene by traditional molecular dynamics model. It is found that water molecules can pass through functional monolayer graphene, but Na^+ and Cl^- are effectively blocked by it, as shown in Fig. 3(c). Koenig *et al.*[40] utilized an ultraviolet-induced oxidative etching technique to create sub-nanometer-sized pores in micrometer-sized graphene crystals and found that the resulting NG membrane can act as an excellent molecular sieve for various gases, as we can see in Fig. 3(d). The results show that the porous membrane can be used to realize effective gas separation. Molecular dynamic simulations have demonstrated that single-layer graphene with nanopores can be efficiently

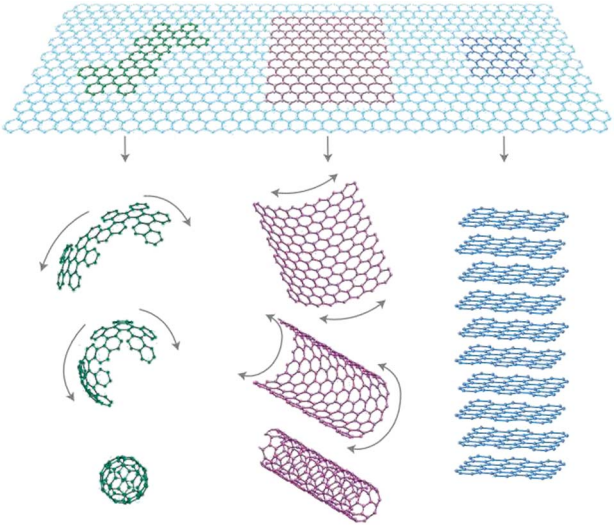

Fig. 2 Graphene is a basic building block for graphitic materials of all other dimensionalities.[23]

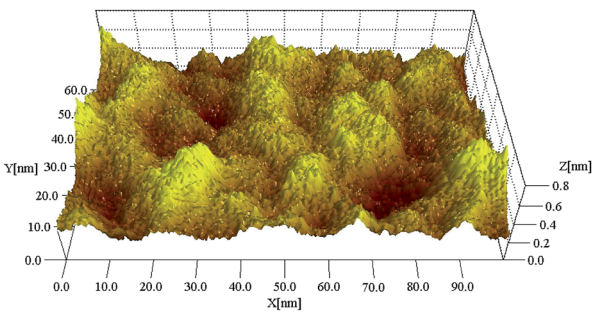

Fig. 1 Image of a single-layer graphene film.[22]

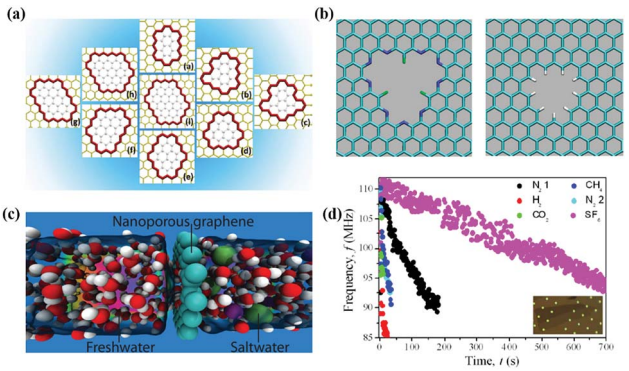

Fig. 3 (a) Structure of porous graphene models; (b) functionalized graphene nanopores: F–N-terminated nanopore (left), H-terminated nanopore (right); (c) graphene can effectively filter NaCl salt from water; (d) frequency of N_2, H_2, CO_2, N_2, CH_4, and SF_6.[37–40]

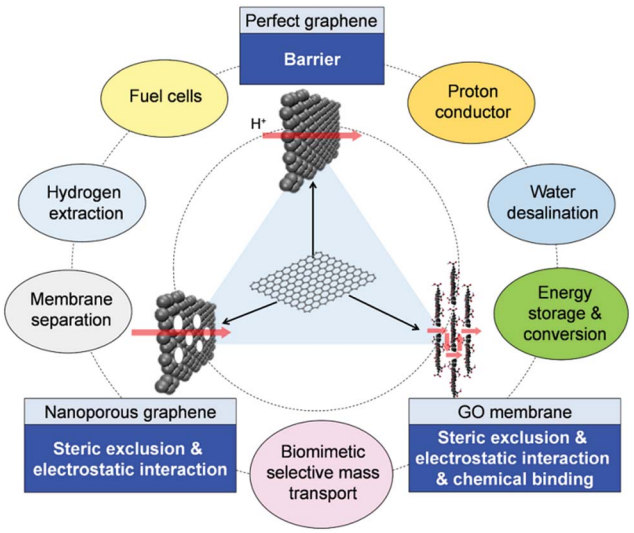

Fig. 4 Schematic illustrating the structure of graphene, NG and GO membrane, the mechanism for selective mass transmembrane transport and possible uses.[52]

utilized for ion rejection and the desalination performance is closely associated to pore structure in terms of size, volume, density, chemical functionalization and operating conditions.[41]

2.3. Structure of graphene-based materials

Graphene oxide (GO) can be easily mass produced through a well-established approach known as Hummers' method.[42] Oxidized graphene sheets have openings and edges that bear hydroxyl, epoxy, and other hydrophilic functional groups and GO has been granted with more accessible porous structures, rendering it with higher ability to adsorb ionic substances.

On the basis of GO, researchers have developed a series of graphene-based materials that contain a variety of active groups or have inorganic nanoparticles loaded on the surface. These modifications give excellent properties to graphene-based materials and these materials are used in specific areas.[43–47] Different research groups have synthesized graphene sheets functionalized with carboxylate, hydroxyl, and amine-terminated polystyrene. These graphene-based materials are used to facilitate ion transport and selective ion rejection.[48–50] In general, surface functionalization can be associated with the formation of new sp^3 carbon network configuration through hybridization of one or more existing sp^2 carbon atoms accompanied by simultaneous loss of electronic conjugation.[51] The graphene monolayers are designed with high recognition principle, so that they can serve as ionic sieves with precisely arranged arrays of functional groups that can efficiently recognize and guide passing ions, as illustrated in Fig. 4.[38]

3. Mass transfer mechanism and adsorption characteristics of graphene-based membranes

For the possible applications in membrane filtration and separation, graphene is also believed to display intriguing properties because of its ultimate thickness and unique electronic cloud structure. The exploration of mass transport and separation properties of graphene is ongoing since 2008, and in the last 2 to 3 years, significant progress has been made in this special research field.[52]

3.1. Transport mechanism of water and gas

Recently, a large amount of research about mass transfer phenomena of graphene-based membranes on gas and water molecules has been confirmed. Nair *et al.*[53] studied the mass transfer of GO membrane, as shown in Fig. 5. They developed a GO membrane of submicron thickness by spin coating, as shown in Fig. 5(a)–(c). The experimental results showed that liquid, steam and gas (including helium) were blocked by the GO membrane completely, as shown in Fig. 5(d) and (e). But the membrane allowed water molecules to flow, as we can see in Fig. 5(f). Based on the above research, in order to explore the phenomenon of water abnormal permeation, Boukhvalov *et al.*[54] created an atomic model of a mixed system of water and GO based on first-principles density functional theory. The research showed that the distance between adjacent layers, which can be controlled either by oxygen reduction or pressure, determined water flow, thus highlighting unique water dynamics in randomly connected two-dimensional spaces. In order to control the channel scale of interlayers, the GO membranes were assembled by different stacking methods and the obtained membranes could achieve different selectivities to gas.[55] At a higher relative humidity, the better connected GO membrane could separate CO_2 and N_2 efficiently. Li *et al.*[56] prepared a GO membrane with structural defects by vacuum filtration and the thickness of the membrane was about 1.8 nm. The prepared membrane could achieve high selectivity of 3400 and 900 for H_2/CO_2 and H_2/N_2 mixed gas, respectively.

3.2. Transport and adsorption mechanisms of ions

Sun *et al.*[57] prepared a GO membrane by drop coating and then studied the permeation behavior of different ions in solution. As shown in Fig. 6(a) and (b), equal volume of salt solution and

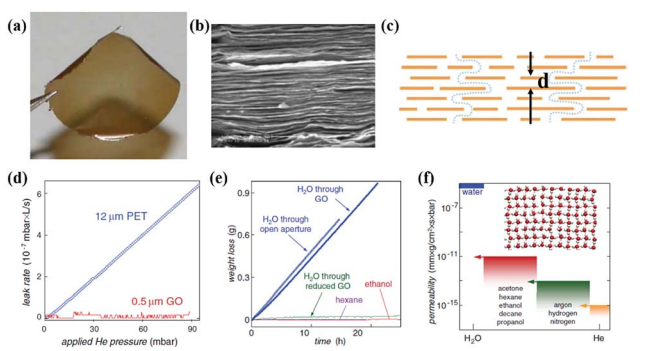

Fig. 5 (a) Photograph of a 1 μm-thick GO film; (b) SEM of the film's cross-section; (c) schematic view for possible permeation; (d) He-leak measurements for a GO membrane and a reference PET film; (e) weight loss for a container sealed with a GO film; (f) permeability of GO with respect to water and various small molecules.[52,53]

deionized water were added to both ends of the GO membrane; as a result, sodium salts permeated quickly, but the heavy metal salts permeated slowly and copper salt and organic compounds were blocked by the membrane. Then they studied the permeation mechanism of the ions, and they tested several salt ions (hydration radius: $Mn^{2+} > Cd^{2+} > Cu^{2+} > Na^{+}$); the test result was $Na^{+} > Mn^{2+} > Cd^{2+} > Cu^{2+}$, which indicates that penetration and hydration radius are not directly related. They also studied permeation mechanism of different salt ions, as shown in Fig. 6(c) and (d).[58,59] The results showed that transition of metal ions tends to interact with oxygen-containing functional groups of GO sheets: the main group of metal ions were more inclined to interact with the sp^2 group *via* π bonds of ions. In summary, it is the different ionic interactions that lead to different ion selectivity, and we can modulate ion transport rate by modifying target functional groups on GO nanosheets.

Graphene-based materials have good adsorption properties to heavy metal ions because of controllable pore structure and high surface area. Huang *et al.*[60] prepared graphene nanosheets by vacuum low temperature stripping method; for these nanosheets, the adsorption of Pb^{2+} in aqueous solution could reach 35 mg g^{-1}. Reduced graphene oxide (rGO) can also adsorb heavy metals ions in water. Leng *et al.*[61] reduced GO by hydrazine; the adsorption of Sb^{3+} by rGO membrane could reach 7.4 mg g^{-1} and adsorption rate was 60%.

3.3. Adsorption of dye molecules

As we all know, dye is one of the important environmental pollution sources. Dye molecules mainly come from the textile printing and paper industry. Moreover, dye has a complex aromatic structure, and physiological toxicity, and it is difficult to biodegrade. Graphene-based materials are a kind of high-quality adsorbent because of their high specific surface area and potential to be widely used in environmental pollution control.

Bradder *et al.*[62] studied the adsorption performance of GO on methylene blue (MB) and malachite green in water; the adsorption capacity was 351 and 248 mg g^{-1}, respectively. Thus, the adsorption property is much higher than that of graphite and activated carbon. In addition, GO has a large number of oxygen functional groups, which play an important role in the adsorption process, and the adsorption mechanism of GO is electrostatic attraction. Yang *et al.*[63] also researched on adsorption performance of GO on MB in water; the adsorption capacity of GO was 714 mg g^{-1}. When the concentration of MB was lower than 250 mg L^{-1}, the adsorption efficiency was higher than 99%. Moreover, under low temperature and high pH conditions, the adsorption of graphene oxide to MB could be accelerated. The study indicated that GO membrane has good adsorption properties for the adsorption of dyes.

4. Method for preparing graphene-based filter membrane

4.1. Vacuum filtration method

The vacuum filtration method is one of the main graphene-based filter membrane preparation methods because of its simple operation. Moreover, it can easily control the thickness of the membrane and has is environment friendly. Vacuum filtration requires the film-forming material to be dispersed in the solvent uniformly, and then the film-forming material be deposited on the substrate under vacuum filtration condition due to fluxion function of solvent molecules. As shown in Fig. 7, Sun *et al.*[64] prepared GO/silver nanoparticle composite membrane by using vacuum filtration method, and cellulose acetate membrane was used as substrate. In addition, the thickness of the membrane was controlled by the volume of the liquid. Wang's group[65] also used this method to prepare GO membrane and they used nanofiber mats to filter graphene oxide solutions; then the as-prepared membrane was dried. Although the vacuum filtration method has the advantage of easy operation, it is difficult to prepare a large-area membrane by this method.

4.2. Layer-by-layer self-assembly method (LBL)

In recent years, with the development of membrane science and technology, layer-by-layer self-assembly technology has become one of the most commonly used methods, as we can see in

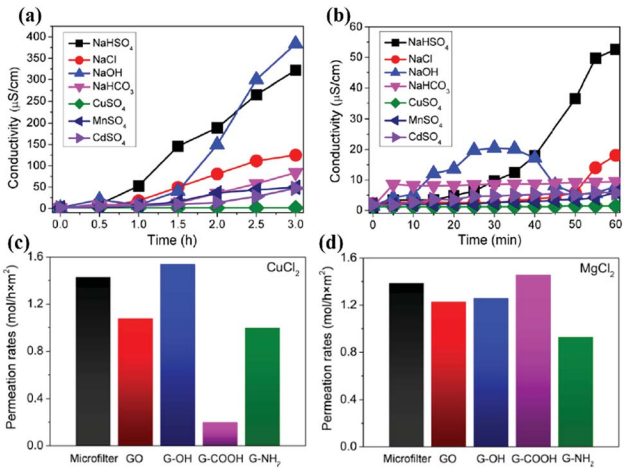

Fig. 6 (a) Penetration processes of different ionic compounds through graphene oxide membranes;[57] (b) initial stages of the penetration processes;[57] (c) Cu^{2+} and (d) Mg^{2+} permeation rates through different membranes.[58,59]

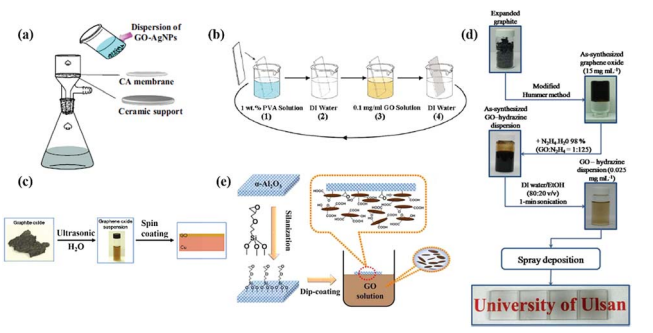

Fig. 7 (a) Vacuum filtration method;[64] (b) layer-by-layer self-assembly method (LBL);[88] (c) spin coating method;[53] (d) spraying method;[71] (e) dip coating method.[74]

Fig. 7(b).[88] It is the electrostatic interaction between ions that acts as the driving force of membrane formation. This method can be used to control the structure and thickness of self-assembled membranes, and we can introduce biologically functional macromolecules, conductive polymers, photosensitive polymers *etc.* into the membrane easily due to nonspecific electrostatic interactions. Like the vacuum filtration method, the layer-by-layer self-assembly (LBL) method is carried out in aqueous solution without any organic solvent, so this method is also environmentally friendly. GO has good hydrophilicity and can be dispersed in water. By contrast, the LBL method is an ideal choice to maintain the stability between the membrane layers *via* covalent bonding and electrostatic interaction.[66] Hu *et al.*[67] prepared GO/poly (allylamine hydrochloride) composite membrane by LBL method *via* electrostatic interaction, which is a new type of water purification membrane. They also prepared GO/trimesoyl chloride (TMC) composite membrane by the same method, which had a good purifying effect on water.[68] Wang's group[69] prepared a new kind of polycation/GO nanofiltration membrane *via* layer-by-layer self-assembly, as shown in Fig. 8. As a result, the anti-swelling property of this novel membrane was enhanced. Also, when the membrane was used to remove dye from water, during the separation of methyl blue molecule from water at 5 bar, the flux and retention rate of the obtained membrane could reach 6.42 kg m^{-2} h^{-1} bar^{-1} and 99.2%, respectively, as we can see in Fig. 9. The LBL method is suitable for preparing a very thin membrane, and the thickness of membrane prepared by this method is uniform.

4.3. Spin coating method

Spin coating is widely used for coating of functional membranes in microelectronics industry. Its equipment is simple and easy to operate, and the thickness of membrane prepared by this method is easy to control. During this method, drying and adjusting of rotational speed are important steps in the preparation of membranes. The thickness of the membrane is adjusted by controlling the time of spin coating, speed of rotation, amount of liquid drop, and concentration and viscosity of the solution. Becerril *et al.*[70] prepared GO membranes by the spin coating method; they used sufficient solution of GO to cover the substrate completely and settle the GO for 60 seconds. At last, GO membrane was obtained under the condition of spin coating at the speed of 500, 800, and 1600 RPM. The coated GO membrane was dried at 100 °C in a vacuum oven and stored in a sealed plastic container. Nair *et al.*[53] also prepared GO membranes by the spin coating method shown in Fig. 7(c). They confirmed that compared with drop coating, the GO membranes obtained by spin coating are more uniform and have a higher transmittance.

4.4. Spraying method

Spraying method is the process of using a professional airbrush to spray a graphene-based solution to a preheated substrate and graphene-based membranes are obtained after solvent evaporation. The function of the spray gun is to disperse the graphene-based solution and form small droplets. The purpose of the preheated substrate is to ensure that the solvent can evaporate rapidly and avoid aggregation of the graphene-based material after deposition of droplets onto the substrate. Pham *et al.*[71] sprayed a mixture of GO solution and hydrazine hydrate solution onto preheated quartz substrates by the spraying method and used nitrogen as the carrier gas for the spray gun system, as we can see in Fig. 7(d). The spraying rate was 3 mL min^{-1} and the distance between the tip of the nozzle and the substrate was 12 cm. The spraying method can be carried out on any substrate and can be easily operated without worrying about damage caused by transfer. This method can be used to prepare large-area membranes, but the uniformity of the membrane is not very good.[72]

4.5. Dip coating method

The dip coating method means soaking the substrate in a solution of graphene-based material, and then the substrate is taken out by a lifting machine after immersion is finished, and the graphene-based membrane is formed on the surface of the substrate after drying. Nguyen[73] prepared hydrophobic graphene membrane by the dip coating method and it was incorporated into a sponge. A rough surface was created between micro/nanoporous hydrophobic graphene nanosheets and sponge, so the sponge could not only maintain their lipophilicity, but also convert from super-hydrophilic to super-

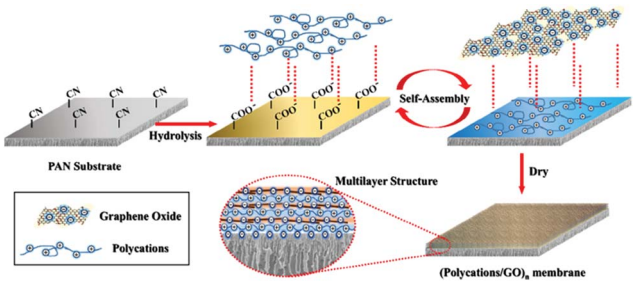

Fig. 8 Schematic of fabrication of polycation/GO NF membrane on PAN substrate *via* LBL self-assembly.[69]

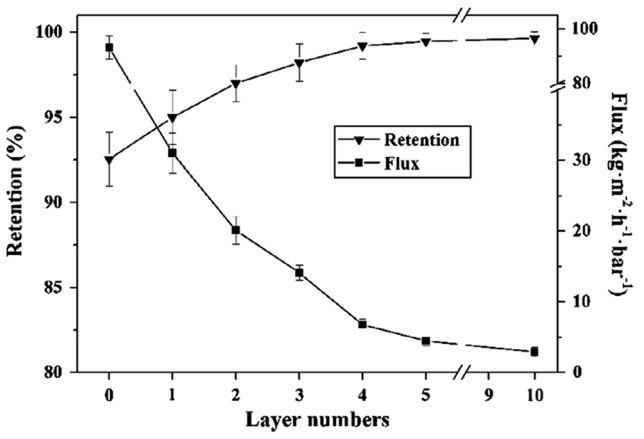

Fig. 9 Effect of layer numbers on separation performance of PDDA/GO membrane.[69]

hydrophobic. The as-prepared sponge could adsorb a variety of grease and organic solvents; in addition, it had high selectivity, good recyclability and a good adsorption capacity, nearly 165 times its own weight. Lou *et al.*[74] used the dip coating method to prepare a GO membrane modified by silane with ceramic as the substrate. Silane modification improved adhesion between GO and ceramic substrate and hydrophilicity of membrane was improved, as shown in Fig. 7(e).

5. Graphene-based/nanometal ultrafiltration membrane

5.1. Graphene-based/silver nanoparticle (AgNP) membrane

It is found that the graphene/AgNP composite membrane has good antibacterial activity, so it can purify water by controlling biological deposition.[75] Sun *et al.*[64] studied the inhibition of *E. coli* by graphene oxide/silver nanoparticle membrane (GO–AgNPs). As shown in Fig. 10, they developed an anti-biofouling membrane by *in situ* fabrication of GO–AgNPs onto cellulose acetate membranes. In this work, *E. coli* was used as a model bacterium to investigate antimicrobial and antifouling properties of the composite membrane due to a growing global concern over the infections caused by this bacterium. The presence of *E. coli* in the feed water affected flux of the membrane. As shown in Fig. 11(a), the flux dropped 88% in 24 h, indicating that the CA membrane can be easily fouled under constant pressure. However, GO–AgNP composite membrane exhibited a better anti-biofouling performance. The flux drop in GO–AgNP composite membrane was only 46%, which is lower than both the GO membrane and Ag membrane. Notably, no *E. coli* was found in the permeate water in the above membrane. Fig. 11(b) shows the population of living cells in the reject water. During filtration, the concentration of living *E. coli*

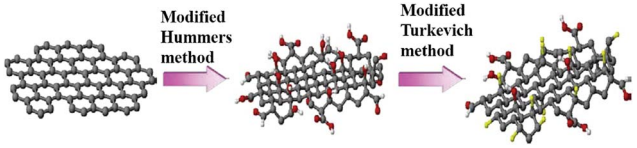

Fig. 10 Mechanism for the formation of GO–AgNPs.[64]

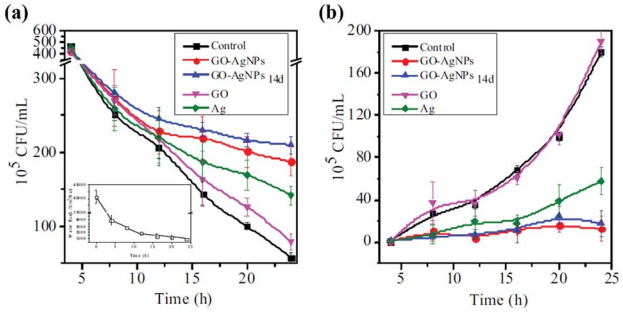

Fig. 11 (a) Flux change using *E. coli*-containing feed water under constant pressure; (b) viable cell concentration in reject water under constant flow rate.[64]

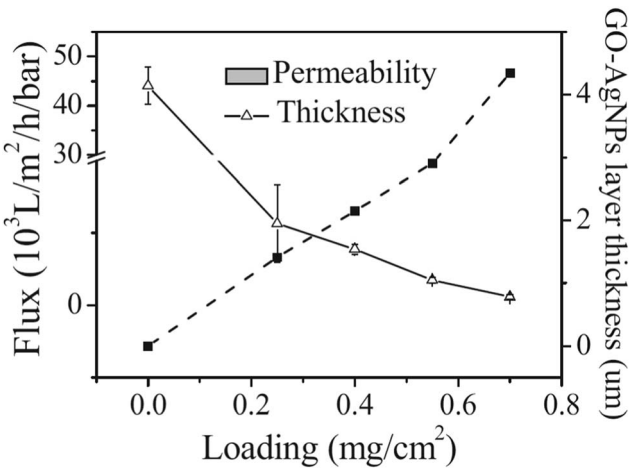

Fig. 12 Variations of GO–AgNP layer thickness and pure water permeability as a function of GO–AgNP loading on membrane.[64]

cells increased to about 200-fold and 190-fold the initial concentration in the reject water at 24 h of filtration when the CA membrane and GO membrane were used, while there was no obvious increase in living *E. coli* cell concentration in the module. These results provided solid evidence that this membrane could inhibit biofilm formation. In addition, as shown in Fig. 12, the water flux of the GO–AgNP membrane was tested, and it was found that the water flux was not affected, but the water flux decreased as film thickness increased.

In order to verify the bacteriostasis of composite membrane, Zeng *et al.*[76] tested its bacteriostatic activity by different test methods. As shown in Fig. 13, they designed a device for inhibiting growth of bacteria by using GO–AgNP membrane. As shown in Table 1, they used GO–AgNPs on the lake for eliminating *E. coli* and coliform; test results showed that GO–AgNP membrane exhibited *E. coli* killing rate of 94%, while the coliform killing rate was 99%, in the creek water, *E. coli* killing rate was as high as 98%. This experiment showed that GO–AgNP membrane had a lethal effect on *E. coli*. This GO–AgNP hydrogel was also tested for real lake and creek water disinfection; the killing rate was more than 94% for *E. coli* cells and around 99%

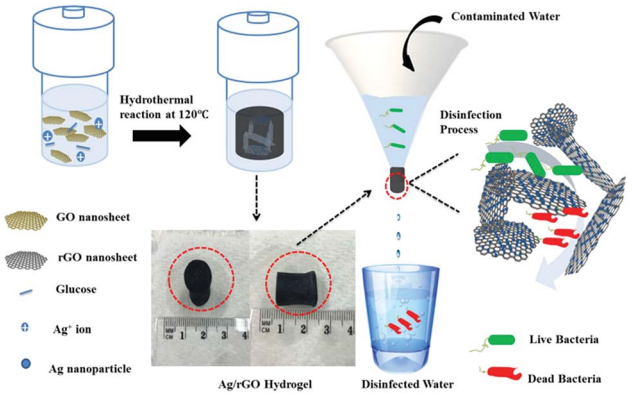

Fig. 13 Synthesis and application of Ag/rGO hydrogel as bactericidal filter for point-of-use water disinfection.[76]

Table 1 *E. coli* and coliform concentration in lake and creek water before and after filtered Ag/rGO hydrogels[76]

	Lake water			Creek water		
[MPN/100 mL]	Original	Treated	Inactivation rate	Original	Treated	Inactivation rate
E. coli	36.4 ± 15.4	<2.0	>94.51% ± 1.16%	153.6 ± 8.0	<2.0	>98.70% ± 0.04%
Coliforms	5308.9 ± 1437.6	15.1 ± 6.5	99.71% ± 0.12%	3295.7 ± 387.6	44.6 ± 23.8	98.71% ± 0.72%

for coliform, showing good feasibility for practical water disinfection. In order to detect the lethality of GO–AgNPs on bacteria and viruses, Song *et al.*[77] compared *E. coli* and *Staphylococcus aureus* (*S. aureus*). As shown in Fig. 14(a), under different pH conditions, it was found that the destruction of *E. coli* by GO–AgNPs was higher than that of *S. aureus*; under a lower pH condition, GO–AgNPs exhibited a more effective antibacterial activity in aqueous solution and the antibacterial activity was more effective against *E. coli* than *S. aureus*. Moreover, enhancement of antioxidants indicated that bacterial cells were in a state of oxidative stress during antibacterial process shown in Fig. 14(b)–(d).

GO–AgNP composite was also found in addition to inhibit and kill bacteria and viruses in sewage. For example, NurulIzriniIkhsan *et al.* found that nitrite ions can be detected in sewage by AgNP membrane.[78] They successfully synthesized a GO–AgNP membrane to detect nitrite in water, as shown in Table 2. Moreover, GO–AgNPs were found to adsorb organic dyes in sewage; Jeyapragasam *et al.*[79] reported that GO–AgNP membrane can adsorb eosin and yellow dyes in waste water. As shown in Fig. 15, in the 303–343 K temperature gradient, the comparison of adsorption degree of eosin yellow between GO and GO–AgNPs shows that adsorption capacity of the latter is much greater. It can be seen that at the same temperature, adsorption capacity of the composite membrane increases with increase in concentration. At the same concentration, the adsorption capacity of the composite membrane increases with increase in temperature. Fig. 16 shows the effect of pH on the adsorption of eosin yellow on GO–AgNP membrane. It was found that at lower pH, adsorption increased sharply with decreasing pH, while at higher pH, adsorption decreased tremendously with increasing pH; electronic repulsion force existed between eosin yellow and GO–AgNPs, which resulted in decrease in adsorption.

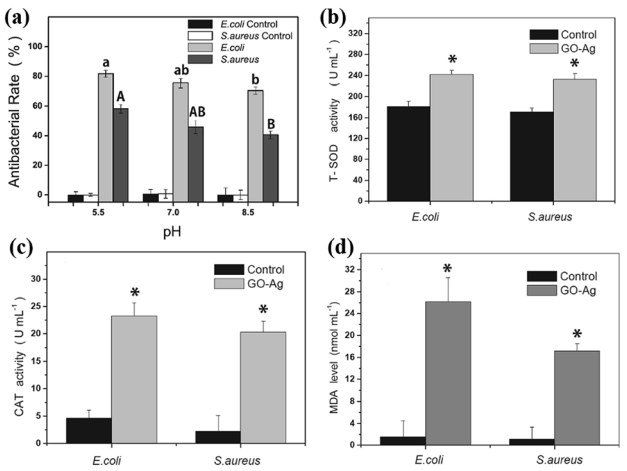

Fig. 14 (a) Effect of pH on antibacterial activity under acidic (pH = 5.5), neutral (pH = 7) and alkaline (pH = 8.5) conditions; changes in intracellular T-SOD (b), CAT activity (c) and content of MDA (d) in cells after exposure to GO–Ag for 20 min compared with the control.[77]

Table 2 Measurement results of nitrite in lake water sample[78]

Sample	Added (μm)	Found (μm)	Recovery (%)
Lake water	10	9.8	98.6
	50	47.8	95.6

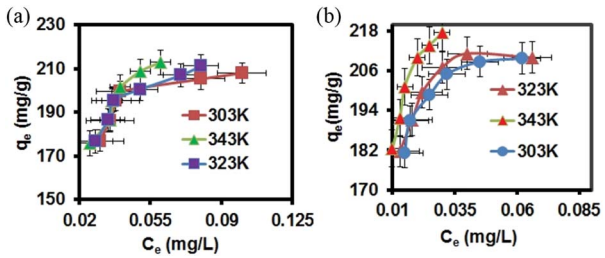

Fig. 15 Plot of adsorption capacity *vs.* equilibrium concentration for adsorption of eosin yellow at three different temperatures and pH onto (a) GO nanosheet and (b) Ag/GO nanocomposite.[79]

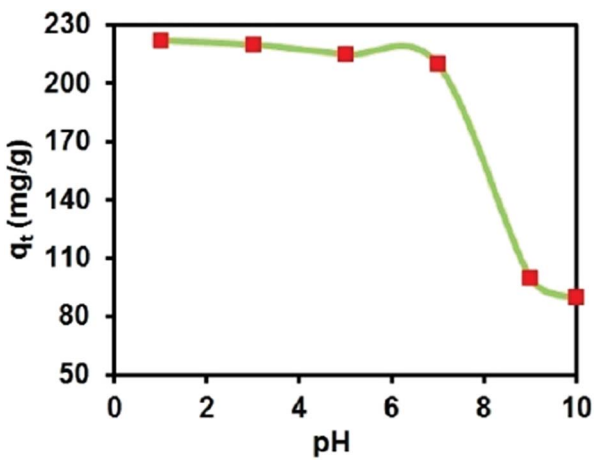

Fig. 16 Effect of solution pH on adsorption capacity.[79]

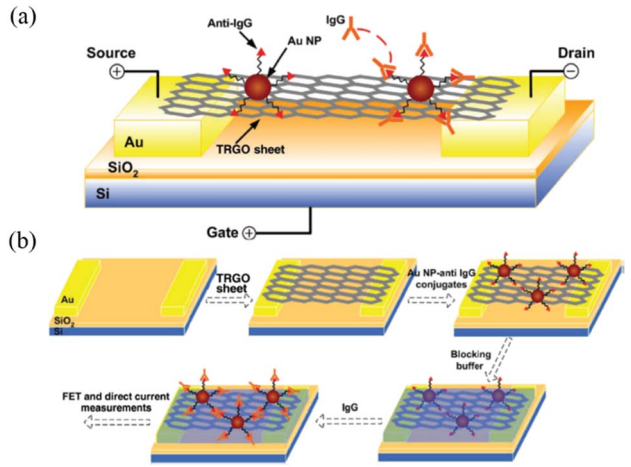

Fig. 17 (a) Schematic of rGO–AuNPs composite FET; (b) schematic of rGO–AuNP composite FET biosensor fabrication.[80]

5.2. Graphene-based/gold nanoparticle (AuNP) ultrafiltration membrane

In addition to loading silver nanoparticle, GO can also form GO–AuNP composites by loading gold nanoparticles. Gold nanoparticles have good biocompatibility and can be assembled with DNA molecules. The optical behavior of gold particles in different states is different, and gold nanoparticles are used to mark DNA in order to trace changes in DNA molecules. Mao *et al.*[80] loaded gold nanoparticles on the surface of rGO for detection of immunoglobulin in antibodies, as shown in Fig. 17. rGO–AuNP composite membrane can also be used for protein detection, thus confirming that the material can be well applied in biomedicine.

GO membranes can also be used as carriers of gold nanoclusters (GNCs) for luminescent agents. Wang *et al.*[81] used HepG2 cells to prove that GNC–rGO membrane can enhance the effect of doxorubicin (DOX). As shown in Fig. 18, DOX-loaded GNC–rGO inhibited HepG2 cell growth more strongly than DOX and GNC–rGO alone, suggesting that DOX was more effectively transported into the cell cytoplasm by the GNC–rGO platform than when used alone. To confirm that GNC–rGO reinforced DOX adsorption by HepG2 cells, they relied on strong spontaneous fluorescence of DOX to follow its distribution in cell cytoplasm after incubation with or without GNC–rGO. DOX alone did not distribute well in the cells, with about half of the DOX molecules resting on the cell membrane surface or in between cells (Fig. 19(a) and (b)). Conversely, when loaded onto GNC–rGO nanocomposites, DOX was well-distributed inside the cells, establishing that GNC–rGO acted as a drug delivery platform that improves DOX internalization by HepG2 cells. This result suggests that the vectorization of GNC–rGO may have enhanced membrane permeability through interactions with phospholipids and/or proteins, resulting in high drug transfer into the cells. Generally speaking, GNC–rGO can become a multimodal probe and drug carrier for targeting, detection, and therapy.

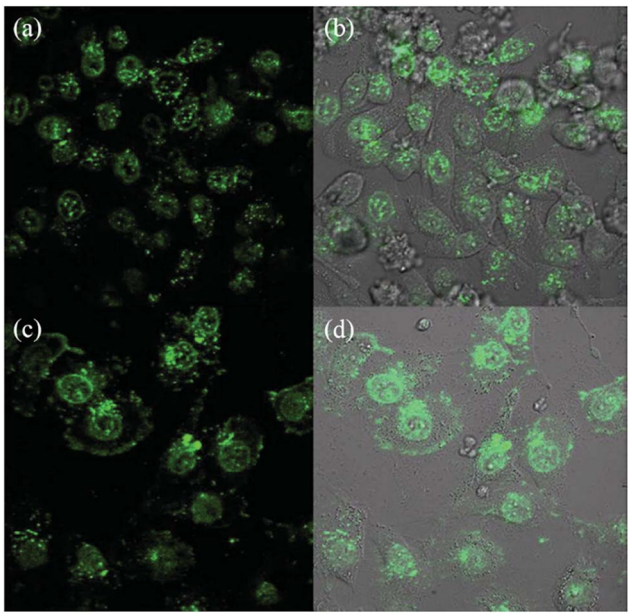

Fig. 19 Laser confocal fluorescence micrographs of HepG2 cells treated with 0.25 mg mL^{-1} DOX (a, b) and DOX-loaded GNC–rGO (c, d)[81]

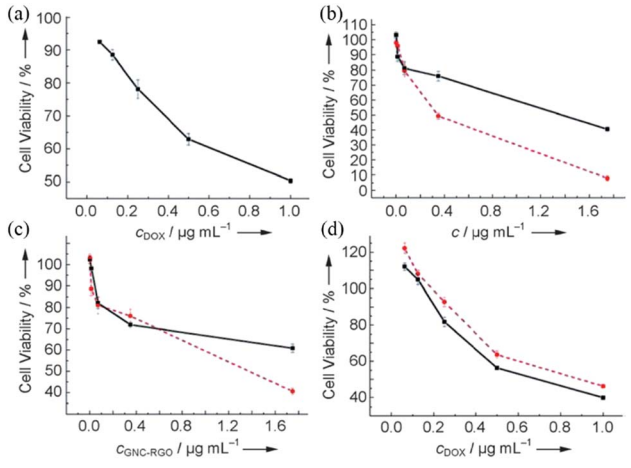

Fig. 18 *In vitro* dose-dependent MTT toxicity tests for HepG2 cells. (a) DOX alone after 24 h incubation; (b) GNCs (red) and GNC/RGO (black) after 48 h incubation; (c) GNC–rGO after 48 h (red) and 72 h incubation (black); (d) DOX-loaded GNC–rGO (black) and DOX alone (red) for HepG2 cells after 48 h incubation.[81]

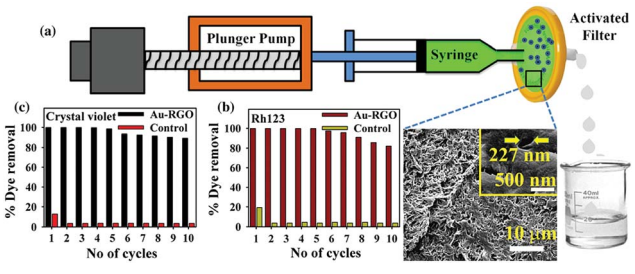

Fig. 20 (a) Schematic of flow device developed for adsorption (inset shows SEM image of filter); (b) and (c) recyclability studies of Rh123 and crystal violet, respectively.[84]

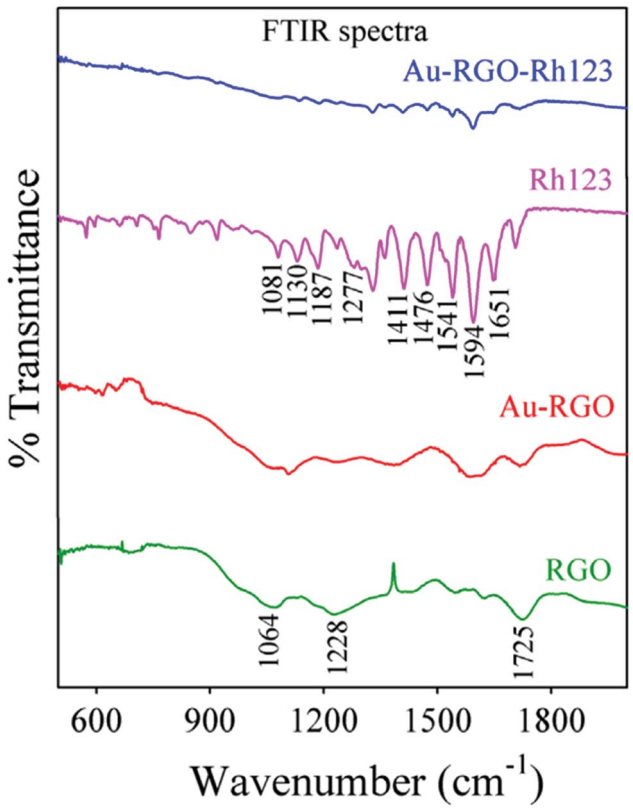

Fig. 21 FTIR spectra of Rh123 before and after adsorption on rGO–Au.[84]

GO–AuNP composite not only has good applications in biomedicine, but also has good applications in water treatment. GO–AuNP composite can adsorb some organic solvents, so it plays a specific role in industrial wastewater treatment.[82,83] As shown in Fig. 20, Prasenjit Kara *et al.*[84] designed a simple device for purifying wastewater by using rGO–AuNP membrane to adsorb Rh123. As shown in Fig. 21, FTIR spectra of rGO exhibit a band at 1725 cm^{-1} corresponding to C=O stretching frequency of the –COOH group. The peak at 1228 cm^{-1} is attributed to C–OH (epoxy functional group) and the peak at 1065 cm^{-1} originates from the C–O band of the alkoxy group. For free Rh123, the peaks at 1651, 1594, 1541, 1476, and 1411 cm^{-1} correspond to xanthene ring stretching frequencies, while those at 1081, 1130, 187 and 1287 cm^{-1} are attributed to C–H bending modes of the xanthene ring. After Rh123 is adsorbed onto rGO–AuNPs membrane, the peaks corresponding to xanthene ring and –COOH, C–OH, and C–O bands of the alkoxy group present in the rGO–AuNPs are perturbed, which indicates interaction of these groups during adsorption. So, the –OH group of rGO–AuNPs undergoes electrostatic interaction with NH^{2+} of Rh123, which may facilitate adsorption of Rh123 onto the rGO–Au surface. Here π–π electrostatic interaction between π electrons of Rh123 and π electrons of rGO–Au nanohybrids may facilitate adsorption of Rh123 onto the rGO–Au surface.

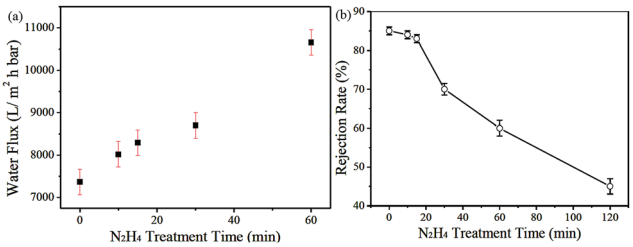

Fig. 23 (a) Water flux and (b) rejection rate of EB molecules of GO/CHNs membrane with N_2H_4 treatment for different durations.[85]

5.3. Other graphene-based/metal ultrafiltration membrane

Although water flux of GO separation membrane is large, molecular rejection rate is high, the pore structure and its distribution of GO separation membrane cannot be effectively controlled. Huang *et al.*[85] used GO as the carrier and copper hydroxide nanowires as templates to prepare nanostrand-channelled GO (NSC-GO) membrane. Fig. 22 shows the schematic of graphene oxide hydroxide ultrafiltration membrane. The membrane had a channel with a diameter of 3–5 nm, which leads to its excellent separation performance. Water flux and rejection rate of Evans blue (EB) molecule were detected, as we can see in Fig. 23; the EB molecular interception rate remained at 84% and the water flux was 695 L m^{-2} h^{-1} bar^{-1}, which is 10 times the water flux of the original GO separation membrane.

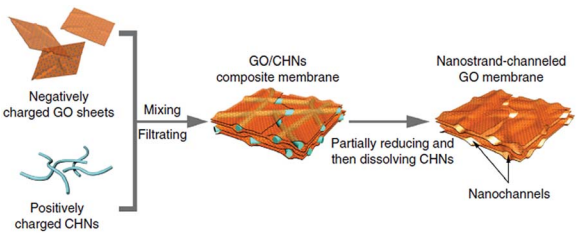

Fig. 22 Fabrication process of GO/CHN membrane and NSC-GO membrane.[85]

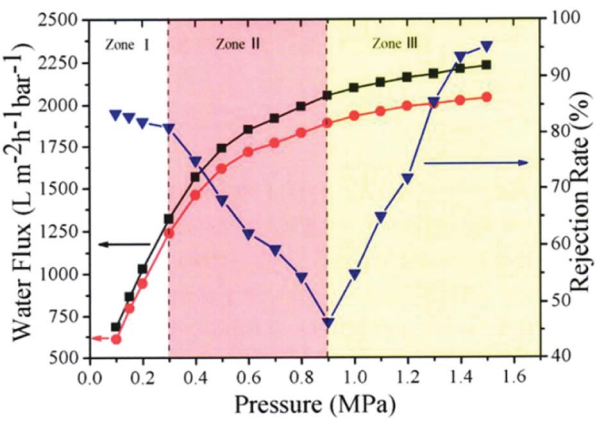

Fig. 24 Pressure-dependent flux and rejection of EB molecules of NSC-GO membrane under different pressure.[85]

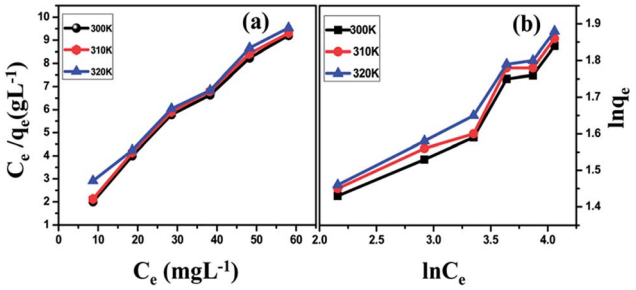

Fig. 25 Adsorption isotherm of Pb ions onto G–Fe_3O_4 surfaces. (a) Langmuir isotherm; (b) Freundlich isotherm. Initial concentration of the ion was 10, 20, 30, 40, 50, and 60 mg L^{-1}; pH = 5; contact time, 120 min and adsorbent dosage 25 mg L^{-1}.[86]

They also tested water flux and EB rejection rate of membranes under different pressure, as shown in Fig. 24; the water flux of GO separation membranes (red curve) increased linearly with increase in pressure. This trend is fully satisfied by the Hagen–Poiseuille equation. As for the rejection rate of membrane, the rejection rate for EB molecules was approximately the same (~83%) in zone I but continuously decreased to 50% in zone II. When the pressure increased further, the rejection rate recovered and reached as high as 95.4% in zone III.

Santhosh *et al.*[86] found that graphene and Fe_3O_4 composite membrane has a good adsorbing effect of heavy metal ions (such as Pb) in wastewater and the adsorption rate increases with the increase in temperature. As shown in Fig. 25, the adsorption rate of Pb at 300 K, 310 K and 320 K increased from 85.2% to 87.2%. They also studied the inhibition of *E. coli* composite membrane killing rate. As shown in Fig. 26, the standard sample for reference, 2 mg mL^{-1} solution of graphene, could reduce 54.11% of *E. coli* and the composite membrane of the same concentration could reduce 92.99% of *E. coli*. To further illustrate the interaction between G–Fe_3O_4 and *E. coli*, the morphology of the cell wall before and after disintegration was characterized by FE-SEM (Fig. 27).

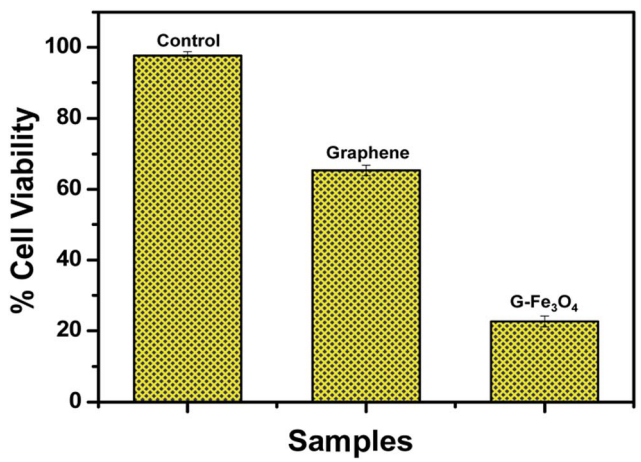

Fig. 26 Cell viability of *E. coli* when treated with graphene and G–Fe_3O_4.[86]

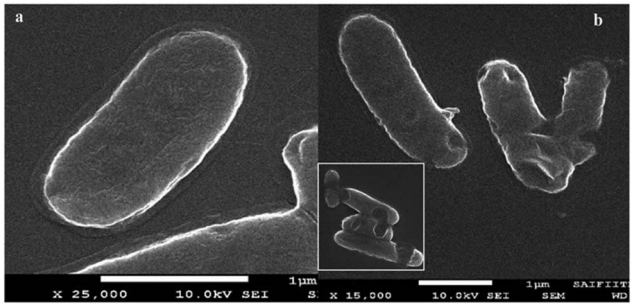

Fig. 27 (a) FE-SEM images of *E. coli* cell control and (b) rupture by G–Fe_3O_4.[86]

Athanasekou[87] found that GO reduction of titanium dioxide (GOT) can effectively adsorb organic dye methyl orange (MO) and methylene blue (MB) in industrial wastewater, and composite membranes with different sizes (GOT-1, GOT-5 and GOT-10) were comparatively evaluated for the removal of both MO and MB under dark and UV light conditions. As a result, GOT-5 exhibited significantly higher adsorption efficiency in the dark compared to the GOT-10 membranes and the adsorption efficiency of GOT-10 was higher than that of GOT-5 under UV irradiation.

6. Conclusion and expectations

In conclusion, membrane separation technology plays an important role in water treatment, food processing, and chemical and pharmaceutical industries. In recent years, many investigations have demonstrated that graphene-based/nanometal composite filter membranes show extraordinary permeation properties, representing the next generation of multifunctional filter membranes in ultrafiltration and nanofiltration applications. The unique two-dimensional structure and excellent hardness of graphene makes it an ideal membrane material. Moreover, a large number of graphene-based materials with different functional groups can be prepared because of active groups on the surface of GO. The resulting graphene-based/nanometal composite membranes exhibit not only water flow enhancement and antimicrobial activity for water purification, but also application prospects for desalination and adsorption of organic dyes.

Although great progress in graphene-based/nanometal composite filter membranes has been achieved, there are still several emerging challenges and opportunities, and some of them are highlighted as follows. (1) Separation and transfer of membranes: as graphene-based/nanometal composite membranes have one- or few-atomic layer thickness, it is difficult to separate and transfer membranes from the substrate. Further study is also needed to separate graphene-based membranes from one substrate and transfer to them other substrates. (2) Mechanical strength of membranes: graphene-based/nanometal composite filter membranes are made up of many small pieces of graphene-based/nanometal composites and there might be insufficient bonding between small pieces.

Much effort should be taken to introduce an interlayer stabilizing force *via* covalent bonding in order to increase mechanical strength of the membrane and prevent dissolution. (3) The membrane spacing can be adjusted by controlling the diameter of nanoparticles or the aspect ratio of nanowires. (4) The number of channels in membranes can be adjusted by controlling the amount of metal particles added. The membrane layer is expanded because of introduction of the nanometal. Therefore, the larger the size of the nanometal, the greater the layer spacing of the membrane, and the more nanometal, the more channels obtained in the membrane. Finally, it cannot be denied that graphene-based membranes, especially graphene-based/nanometal membranes, are promising enough to act as next-generation multifunctional filtration and separation membranes, whose performance and functions are superior to state-of-the-art polymer- and ceramics-based membranes.

Conflicts of interest

There are no conflicts to declare.

Acknowledgements

This work was supported by the (1) Natural Scientific Foundation of China (Grant no. 51641204, 51503112, 51373081), Natural Scientific Foundation of Shandong Province (Grant no. ZR2015EM008), Key Research and Development Plan of Shandong Province (Grant no. 2017GGX20112); (2) the Program for Introducing Talents of Discipline to Universities ("111" plan); (3) The National One-Thousand Foreign Expert Program (Grant No. WQ20123700111); (4) State Key Project of International Cooperation Research (2016YFE0110800); (5) The 1st Level Discipline Program of Shandong Province of China.

Notes and references

1 M. Elimelech and W. A. Phillip, *Science*, 2011, **333**, 712–717.
2 M. T. M. Pendergast and E. M. V. Hoek, *Energy Environ. Sci.*, 2011, **4**, 1946–1971.
3 M. Nyström, L. Kaipia and S. Luque, *J. Membr. Sci.*, 1995, **98**, 249–262.
4 C. K. Diawara, *Sep. Purif. Rev.*, 2008, **37**, 302–324.
5 A. L. Ahmad, L. S. Tan and S. R. Shukor, *J. Hazard. Mater.*, 2008, **151**, 71–77.
6 Y. Zhang, C. Causserand and P. Aimar, *Water Res.*, 2006, **40**, 3793–3799.
7 D. L. Nghiem and I. A. Schäfer, *Sep. Sci. Technol.*, 2005, **40**, 2633–2649.
8 L. D. Nghiem, A. Manis and K. Soldenhoff, *J. Membr. Sci.*, 2004, **242**, 37–45.
9 K. Kimura, G. Amy and J. E. Drewes, *J. Membr. Sci.*, 2003, **227**, 113–121.
10 K. O. Agenson, J. I. Oh and T. Urase, *J. Membr. Sci.*, 2003, **225**, 91–103.
11 P. S. Shi, T. A. Hatton and Y. C. Sui, *J. Membr. Sci.*, 2012, **401–402**, 152–162.
12 K. S. Novoselov, A. K. Geim, S. V. Morozov, D. Jiang and Y. Zhang, *Science*, 2004, **306**, 666–669.
13 S. K. Georgantzinos, G. I. Giannopoulos and N. K. Anifantis, *Mater. Des.*, 2010, **3**, 4646–4654.
14 H. K. Chae, D. Y. Siberio-Pérez, J. Kim, Y. Go, M. Eddaoudi, A. J. Matzger, M. O'Keeffe and O. M. Yaghi, *Nature*, 2004, **427**, 523–527.
15 Y. C. Zhao, L. J. Huang and Y. X. Wang, *J. Alloys Compd.*, 2016, **687**, 95–103.
16 A. Geim, P. Kim and K. Novoselov, *Science*, 2007, **315**, 1379.
17 Z. Jiang, Y. Zhang and Y. W. Tan, *Solid State Commun.*, 2007, **143**, 14–19.
18 B. Jabakhanji, C. Consejo and N. Camara, *J. Phys. D: Appl. Phys.*, 2014, **47**, 245–248.
19 Y. Zhang, Y. Tan, H. L. Stormer and P. Kim, *Nature*, 2005, **438**, 201–204.
20 Y. Wang, Y. Huang and Y. Song, *Nano Lett.*, 2009, **9**, 220–224.
21 X. Huang, X. Qi and F. Boey, *Chem. Soc. Rev.*, 2012, **41**, 666–686.
22 L. J. Huang, Y. X. Wang and J. G. Tang, *J. Alloys Compd.*, 2016, **694**, 1140–1148.
23 K. Falk, F. Sedlmeier and L. Joly, *Nano Lett.*, 2010, **10**, 4067.
24 T. Kuila, S. Bose and A. K. Mishra, *J. Mater. Sci.*, 2012, **57**, 1061–1105.
25 Y. Zhu, S. Murali, W. Cai, X. Li, J. W. Suk, J. R. Potts and R. S. Ruof, *Adv. Mater.*, 2010, **22**, 3906–3924.
26 V. Singh, D. Joung and Z. Lei, *Prog. Mater. Sci.*, 2011, **56**, 1178–1271.
27 X. Guo, W. Liu and L. Cao, *Appl. Surf. Sci.*, 2013, **283**, 498–504.
28 X. Dong, Q. Long and J. Wang, *Nanoscale*, 2011, **3**, 5156–5160.
29 X. Yang, C. Cheng and Y. Wang, *Science*, 2013, **341**, 534–537.
30 T. S. Sreeprasad, S. M. Maliyekkal and K. P. Lisha, *J. Hazard. Mater.*, 2011, **186**, 921.
31 T. Wu, Q. Xue and C. Ling, *J. Phys. Chem. C*, 2012, **118**, 7369–7376.
32 R. K. Josh, P. Carbone, F. C. Wang, V. G. Kravets, Y. Su, I. V. Grigorieva, H. A. Wu, A. K. Geim and R. R. Nair, *Science*, 2014, **343**, 752–754.
33 S. Ansari and E. P. Giannelis, *J. Polym. Sci., Part B: Polym. Phys.*, 2010, **47**, 888–897.
34 H. Fan, L. Wang and K. Zhao, *Biomacromolecules*, 2010, **11**, 2345–2351.
35 K. Zhang, L. L. Zhang and X. S. Zhao, *Chem. Mater.*, 2010, **22**, 1392–1401.
36 T. Kuila, S. Bose and C. E. Hong, *Carbon*, 2011, **49**, 1033–1037.
37 H. Du, J. Li and J. Zhang, *J. Phys. Chem. C*, 2011, **115**, 23261–23266.
38 K. Sint, B. Wang and P. Král, *J. Am. Chem. Soc.*, 2008, **130**, 16448.
39 D. Cohentanugi and J. C. Grossman, *Nano Lett.*, 2012, **12**, 3602–3608.
40 S. P. Koenig, L. Wang and J. Pellegrino, *Nat. Nanotechnol.*, 2012, **7**, 728.

41 B. Tüzün and Ş. Erkoç, *J. Comput. Theor. Nanosci.*, 2013, **10**, 470–480.
42 W. S. Hummers and R. E. Offeman, *J. Am. Chem. Soc.*, 1958, **80**, 1339.
43 S. N. Ariffin, H. N. Lim and F. A. Jumeri, *Ceram. Int.*, 2014, **40**, 6927–6936.
44 E. Yoo, T. Okata and T. Akita, *Nano Lett.*, 2009, **9**, 2255–2259.
45 J. Zhao, S. Pei and W. Ren, *ACS Nano*, 2010, **4**, 5245–5252.
46 X. Yang, Y. Ma, Y. Huang, Y. Wang and Y. Chen, *J. Mater. Chem.*, 2009, **19**, 2710–2714.
47 G. M. Scheuermann, L. Rumi and P. Steurer, *J. Am. Chem. Soc.*, 2009, **131**, 8262–8270.
48 D. Konatham, J. Yu and T. A. Ho, *Langmuir*, 2013, **29**, 11884–11897.
49 B. Konkena and S. Vasudevan, *J. Phys. Chem. Lett.*, 2012, **3**, 867–872.
50 E. Y. Choi, T. H. Han and J. Hong, *Mater. Chem.*, 2010, **20**, 1907–1912.
51 H. Wang, X. Yuan and Y. Wu, *Adv. Colloid Interface Sci.*, 2013, **195–196**, 19–40.
52 P. Sun, K. Wang and H. Zhu, *Adv. Mater.*, 2016, **28**, 2287.
53 R. R. Nair, H. A. Wu and P. N. Jayaram, *Science*, 2012, **335**, 442–444.
54 D. W. Boukhvalov, M. I. Katsnelson and Y. W. Son, *Nano Lett.*, 2013, **13**, 3930–3935.
55 H. W. Kim, H. W. Yoon and S. M. Yoon, *Science*, 2013, **342**, 91–95.
56 H. Li, Z. Song and X. Zhang, Ultrathin, *Science*, 2013, **342**, 95–98.
57 P. Sun, M. Zhu and K. Wang, *ACS Nano*, 2013, **7**, 428–437.
58 P. Sun, H. Liu and K. Wang, *J. Phys. Chem. C*, 2014, **118**, 19396–19401.
59 P. Sun, F. Zheng and M. Zhu, *ACS Nano*, 2014, **8**, 850–859.
60 Z. H. Huang, X. Zheng and W. Lv, *Langmuir*, 2011, **27**, 7558–7562.
61 Y. Leng, W. Guo and S. Su, *Chem. Eng. J.*, 2012, **211–212**, 406–411.
62 P. Bradder, S. K. Ling and S. Wang, *J. Chem. Eng. Data*, 2011, **56**, 138–141.
63 S. T. Yang, S. Chen and Y. Chang, *J. Colloid Interface Sci.*, 2011, **359**, 24–29.
64 X. F. Sun, J. Qin and P. F. Xia, *Chem. Eng. J.*, 2015, **281**, 53–59.
65 J. Wang, P. Zhang and B. Liang, *ACS Appl. Mater. Interfaces*, 2016, **8**, 6211–6218.
66 M. Baoxia, *Science*, 2014, **343**, 740–742.
67 M. Hu and B. Mi, *J. Membr. Sci.*, 2014, **469**, 80–87.
68 M. Hu and B. Mi, *Environ. Sci. Technol.*, 2013, **47**, 3715–3723.
69 L. Wang, N. Wang and J. Li, *Sep. Purif. Technol.*, 2016, **160**, 123–131.
70 H. A. Becerril, J. Mao and Z. Liu, *ACS Nano*, 2008, **2**, 463–470.
71 V. H. Pham, T. V. Cuong and S. H. Hur, *Carbon*, 2010, **48**, 1945–1951.
72 H. F. Shi, C. Wang and Z. P. Sun, *Sci. China: Phys., Mech. Astron.*, 2015, **58**, 1–5.
73 D. D. Nguyen, N. H. Ta and S. B. Lee, *Energy Environ. Sci.*, 2012, **5**, 7908–7912.
74 Y. Lou, G. Liu and S. Liu, *Appl. Surf. Sci.*, 2014, **307**, 631–637.
75 H. L. Yang, J. C. Lin and C. Huang, *Water Res.*, 2009, **43**, 3777–3786.
76 X. Zeng, D. T. Mccarthy and A. Deletic, *Adv. Funct. Mater.*, 2005, **25**, 4344–4351.
77 B. Song, Z. Chang and G. Zeng, *Arch. Biochem. Biophys.*, 2016, **604**, 167.
78 N. I. Ikhsan, P. Rameshkumar and A. Pandikumar, *Talanta*, 2015, **144**, 908–914.
79 T. Jeyapragasam, *Mater. Today*, 2016, **3**, 2146–2154.
80 S. Mao, G. Lu and K. Yu, *Adv. Mater.*, 2010, **22**, 3521–3526.
81 C. Wang, J. Li and C. Amatore, *Angew. Chem., Int. Ed.*, 2011, **50**, 11644–11648.
82 S. Thakur and N. Karak, *Carbon*, 2012, **50**, 5331–5339.
83 J. Sarkar, J. Chowdhury and P. Pal, *Vib. Spectrosc.*, 2006, **41**, 90–96.
84 P. Kara, S. Sardar and B. Liu, *Sci. Technol. Adv. Mater.*, 2016, **17**, 375–386.
85 H. Huang, Z. Song and N. Wei, *Nat. Commun.*, 2013, **4**, 2979.
86 C. Santhosh, P. Kollu and S. Doshi, *RSC Adv.*, 2014, **4**, 28300–28308.
87 C. P. Athanasekou, S. Morales-Torres and V. Likodimos, *Appl. Catal., B*, 2014, **158–159**, 361–372.
88 X. Zhao, Q. Zhang, Y. Hao, Y. Li, Y. Fang and D. Chen, *Macromolecules*, 2010, **43**, 9411–9416.